### 2.3.2. GDT Reconstruction Algorithm

The goal of tomographic reconstruction algorithms is to convert average quantities along paths passing through the testbed into the spatial variation of the quantity throughout the region of interest. In general, many "projections" (groups of paths lying in a plane and sharing either a common origin or a common direction) are required to produce an accurate reconstruction of the spatial variation within this plane. Three-dimensional variations are then built up from multiple planes. Under the simplifying assumption of an axisymmetric spatial variation within a plane, only one projection is required since the field appears the same when viewed from different angular directions.

The Abel transform (cf. Vest, 1985) can be used to reconstruct the axisymmetric spatial variation of a function $f(r, R)$ from its line integral $g(x, R)$ along the path in the $y$ direction at horizontal position $x$, as shown in Figure 18.

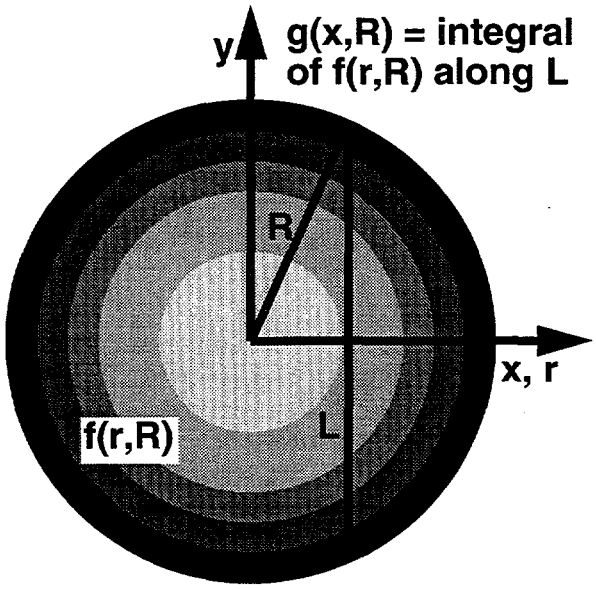


Figure 18. Schematic diagram of Abel transform geometry.

With these definitions, the Abel transform relates $f(r, R)$ and $g(x, R)$ in the following manner:

$$g(x,R) = 2\int_0^{\sqrt{R^2-x^2}} f(\sqrt{x^2+y^2}, R)dy = 2\int_x^R \frac{f(r,R)r}{\sqrt{r^2-x^2}}dr\,,\; f(r,R) = -\frac{1}{\pi}\int_r^R \frac{(dg/dx)}{\sqrt{x^2-r^2}}dx\,. \qquad (12)$$

A quantity that arises naturally in axisymmetric tomography is $\psi$, the "path-averaged" value of $f$:

$$\psi(x,R) = \frac{g(x,R)}{2\sqrt{R^2-x^2}}, \qquad (13)$$

which is the line integral of $f$ along the path at $x$ divided by the path length. The functions $f$ and $\psi$ have a remarkable property that is useful to Abel tomographic reconstruction algorithms: if one function is an even polynomial, then the other function is also an even polynomial of the same degree.

For the representations

$$f(r,R) = \sum_{m=0}^{N} a_m (r/R)^{2m}, \quad \psi(x,R) = \sum_{n=0}^{N} b_n (x/R)^{2n}, \tag{14}$$

the following reconstruction relations are obtained:

$$a_m = \sum_{n=0}^{N} c_{mn} b_n, \quad b_n = \sum_{m=0}^{N} d_{nm} a_m, \tag{15}$$

where in terms of binomial coefficients

$$c_{mn} = \begin{cases} -\left[\dfrac{2m+1}{2^{2n}(2n-2m-1)}\right]\binom{2n-2m}{n-m}\binom{2m}{m}, & m \le n \\ 0, & m > n \end{cases}, \tag{16}$$

$$d_{nm} = \begin{cases} \left[\dfrac{2^{2n}}{2m+1}\right]\binom{2m-2n}{m-n}\Big/\binom{2m}{m}, & n \le m \\ 0, & n > m \end{cases}. \tag{17}$$

GDT data are acquired and analyzed in the following manner. The attenuation field is the quantity of interest and is assumed to be axisymmetric, which is usually a good approximation for time-averaged bubble-column flow. Given the assumption of axisymmetry, reconstruction of the radial variation of the attenuation coefficient requires only one projection: the intensities $I_i$ are measured at a series of horizontal source-detector positions $x_i$ while the vertical source-detector position $z$ is held constant. To acquire the data needed to reconstruct the phase volume fraction spatial variations, this type of data is acquired for three different circumstances. First, a scan is performed with the column "empty" (i.e. empty of liquid but full of gas). Second, a scan is performed with the column "full" (i.e. full of liquid but empty of gas). Third, additional scans are performed with the gas-liquid multiphase flow at the desired conditions. The following expressions then relate $f$ and $\psi$ to the attenuation coefficient $\mu$:

$$f = \frac{\mu - \mu_G}{\mu_L - \mu_G}, \quad \psi = \frac{\ln(I^{\text{empty}}) - \ln(I^{\text{flow}})}{\ln(I^{\text{empty}}) - \ln(I^{\text{full}})}. \tag{18}$$

Tomographic reconstruction proceeds in the following manner.

1. Measure the values $\psi_i$ on a set of paths $x_i$.
2. Fit the $\{(x_i, \psi_i)\}$ with even powers of $x_i/R$ to find the $b_n$.
3. Use the $c_{mn}$ to find the $a_m$ and the normalized attenuation radial variation $f$.

Note that for a two-phase gas-liquid flow, $f$ is equal to the liquid volume fraction $\varepsilon_L$ in the medium and hence is zero for pure gas and unity for pure liquid. In a three-phase flow, additional information is needed to relate $f$ to the phase volume fractions.

## 2.4. Electrical-Impedance Tomography (EIT) Technique

Another method of characterizing material distribution is electrical-impedance tomography (EIT). EIT techniques have been discussed extensively in the recent review by Ceccio and George (1996). The underlying physical basis of EIT is the assumption that the impedance of a mixture can be sensibly related to the volume fractions and impedances of the materials comprising the mixture so that spatially resolved impedance measurements yield information about the spatial distribution of the materials in the mixture. If a gas-liquid mixture is considered where the gas is insulating and the liquid is purely resistive with conductivity $\sigma_L$, the Maxwell-Hewitt relation for a random dispersion of small insulating spheres (gas bubbles) within a continuum (the liquid) relates the mixture conductivity $\sigma_m$ to the gas volume fraction $\varepsilon_G$ (cf. Hewitt, 1978; Ceccio and George, 1996):

$$\sigma_m/\sigma_L = \frac{1-\varepsilon_G}{1+(1/2)\varepsilon_G}, \quad \varepsilon_G = \frac{1-(\sigma_m/\sigma_L)}{1+(1/2)(\sigma_m/\sigma_L)}. \tag{19}$$

Figure 19 shows a schematic diagram of a generic EIT setup. A region of material is surrounded by an insulating boundary on which several electrodes are mounted. A known current is injected into the material from one electrode and is withdrawn from another, and voltages are measured at all electrodes (both current-carrying and those that carry no current). This process is repeated for different pairs of electrodes until all combinations of electrodes have been examined. Tomographic reconstruction techniques are subsequently applied to determine the spatial variation of the electrical conductivity of the medium under examination. Note that reconstruction algorithms are necessarily considerably more complex for EIT than for GDT: the current paths through the material depend on the impedance distribution, whereas the gamma-photon paths through the material are known a priori since they are independent of the material distribution.

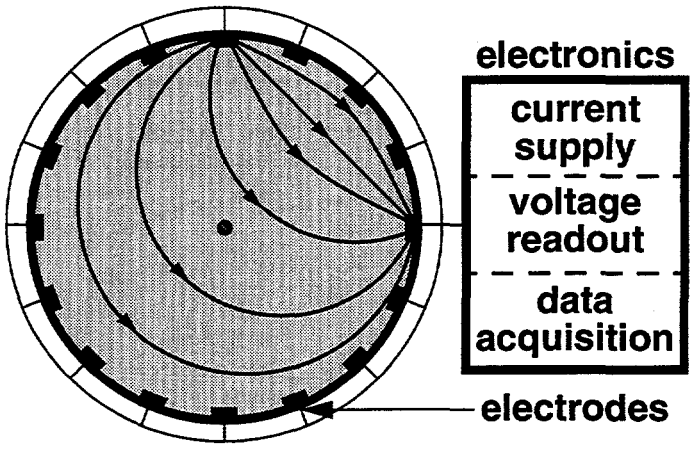


Figure 19. Schematic diagram of electrical-impedance tomography (EIT).

The methodology, efficiency, and accuracy of various EIT techniques continue to be a subject of research (e.g. Barber et al., 1983; Yorkey et al., 1987; Webster, 1990; Hua and Woo, 1990; Jones et al., 1993; Lin et al., 1993; O'Hern et al., 1995ab; Dickin and Wang, 1996; Loh and Dickin, 1996; Savolainen et al., 1996; Torczynski et al., 1996b; Shollenberger et al., 1997b; Mann et al., 1997). EIT techniques can be broadly grouped in terms of the problem dimensionality (2 or 3), the impedance model employed (e.g., resistive, capacitive), the numerical method used to discretize the equations

(e.g., finite-element method, boundary-element method), the representation of the impedance field (e.g., piecewise constant, exponential), the means by which the impedance field is modified during an iteration (e.g., back-projection between equipotential lines, Newton-Raphson), and the intended application (e.g., biomedical imaging, multiphase flow measurement).

The purpose of the present study is to implement an EIT technique suitable for making spatially resolved measurements of gas volume fraction in gas-liquid bubble-column flow. The medium is taken to be purely conducting (no capacitive effects), which is reasonable for polar liquids like water and which facilitates both hardware and software development. In contradistinction to the work of Lin et al. (1993), the emphasis here is not on the accurate determination of arbitrary gas-liquid interfaces or other sharp discontinuities in electrical properties. Instead, the medium under consideration (a continuum liquid phase within which a very large number of small gas bubbles are dispersed) is assumed to have smoothly varying electrical properties when averaged over length scales large compared with the bubble size and separation but small compared with the extent of the medium. Since variations of macroscopic quantities is gradual in the vertical direction for bubble-column flow, the electrical properties of the medium are assumed to have no variation in this direction, so the technique is two-dimensional, at least in this sense. Two reconstruction techniques have been examined: one employing a finite-element method with a Newton-Raphson scheme for minimization and the other employing a boundary-element method with Powell minimization.

### 2.4.1. EIT System

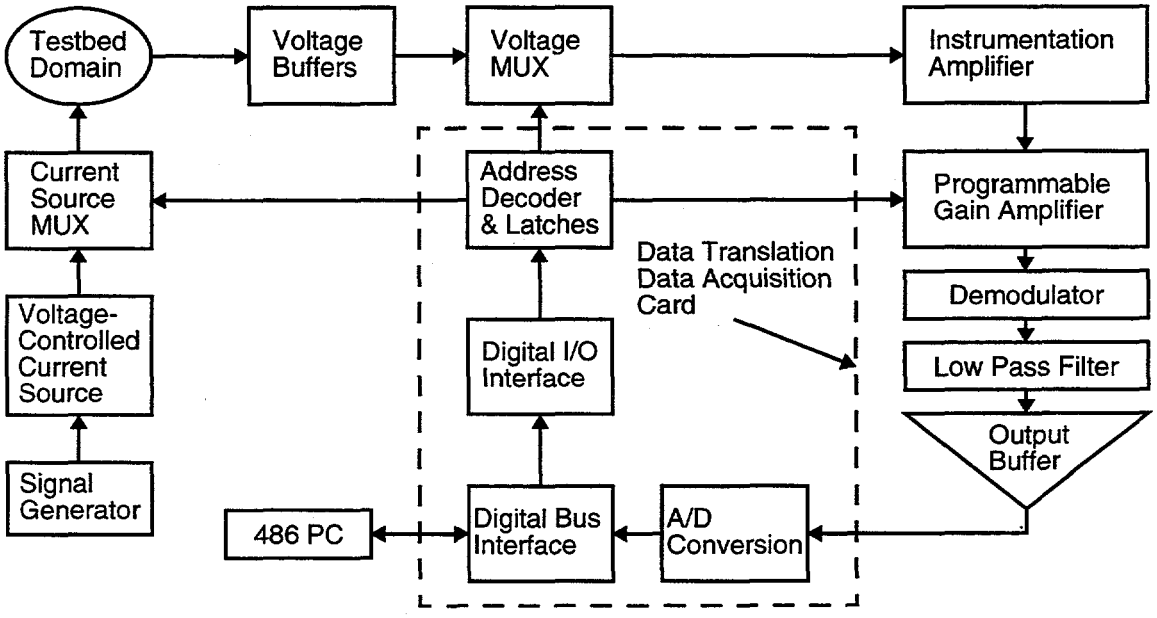


Figure 20. Block diagram of EIT hardware.

The EIT system developed herein consists of an electrode array mounted on a probe ring, a signal generator, a voltage-controlled current source (VCCS), multiplexers (MUXes) to and from the electrode array, an instrumentation amplifier, phase-sensitive demodulators, and a digital controller. A block diagram of the system is shown in Figure 20. The EIT system sources and sinks current at two ports, and voltages at all ports are measured relative to the sink port. The domain is excited with

a 50 kHz AC electric field, a frequency acceptable for air-water systems (cf. Ceccio and George, 1996). The injection current is created by a VCCS employing two operational amplifiers in a positive feedback design. Extremely high domain impedances should be avoided to prevent saturation of the VCCS. To acquire a set of projections with a good signal-to-noise ratio, significant current should be induced within the entire domain so as to produce measurable changes in the boundary voltages. This can be achieved by requiring a complete EIT measurement to utilize all distinct pairs of ports (without regard to order) as the source and sink ports. For $N_e$ electrodes in the EIT setup, a complete EIT measurement consists of measuring the voltages $v_k^{(mn)}$ at all electrodes $k$ for all $N_e(N_e-1)/2$ distinct pairwise combinations $(mn)$ of electrodes, where electrodes $m$ and $n$ are the source and the sink. Thus, a complete measurement yields $N_e^2(N_e-1)/2$ voltage measurements. However, only $N_e(N_e-1)/2$ pieces of information are obtained, which correspond to the maximum number of independent resistors needed to describe an $N_e$-port resistive network (cf. Ceccio and George, 1996).

The electrode array is connected to the current source and sink via analog MUXes. MUXes are also used to connect the electrode array to the differential amplifier used to measure electrode voltages. Coaxial cable is used to carry the injection current to and from the electrodes surrounding the domain, and the shields of the cable are brought to the electrode voltage with voltage followers. A separate set of cables is used to connect the electrodes to the voltage MUXes to prevent the inclusion of any voltage drop occurring across the current lines, and the voltages on each electrode are buffered with a single operational amplifier. These voltage signals are passed to a differential amplifier which is used to measure the difference between the voltages on two electrodes. The differential amplifier has a good common mode rejection ratio (CMRR) and allows the measurement of voltage differences over a wide dynamic range.

The signal from the differential amplifier is demodulated with a phase-sensitive demodulator (PSD). Two demodulators are used to recover the in-phase and quadrature portion of the signal amplitude. The in-phase and quadrature demodulator output is low-pass filtered with a cutoff frequency of 25 kHz. The two voltage outputs of the PSD are then buffered and passed to the analog-to-digital converter on the digital controller board. A digital controller is used to select the current injection electrodes and perform the voltage measurements as well as acquire the demodulated signal levels. The data acquisition rate is 200 kHz, so the signal must be sampled at least four times to capture one period. Voltages are typically measured 64 times at each electrode to ensure an accurate average. An analog/digital interface is used to connect a PC to the EIT system.

The EIT system herein employs 16 electrodes, and these electrodes are placed at equal azimuthal intervals around the inner perimeter of a lucite cylindrical sections referred to as probe rings. The probe rings fabricated for this study have an inner diameter of 19.05 cm (7.5 inch) and can be used in two configurations, shown in Figure 21. If the ends are capped off, a probe ring can be used to study static objects immersed in water for validation experiments. If installed in a gas-liquid bubble column, a probe ring can be used to measure the material spatial distribution of a multiphase flow. Two types of electrodes have been employed, as shown in Figure 21: 0.25 inch $\times$ 3.0 inch strips of 0.003 inch-thick stainless steel referred to as strip electrodes, and 3 mm (0.125 inch) disks referred to as point electrodes. The principal advantage of using strip electrodes is that two-dimensional electric fields are obtained if the strip lengths are at least twice the probe ring diameter and if the conductivity field does not vary along the length of the strips. Unfortunately satisfying the first condition typically falsifies the second condition. Thus, three-dimensional solutions for the electric field are required, so point electrodes are preferred because they minimize the extent of the domain required by computational simulations. The principal disadvantages of point electrodes are that somewhat larger voltages are required to achieve the same current flow and that somewhat lower sensitivity is achieved. These are partially offset, however, by ease of construction, mounting, and alignment, high mechanical integrity even during vigorous flow, and good size-scaling properties.

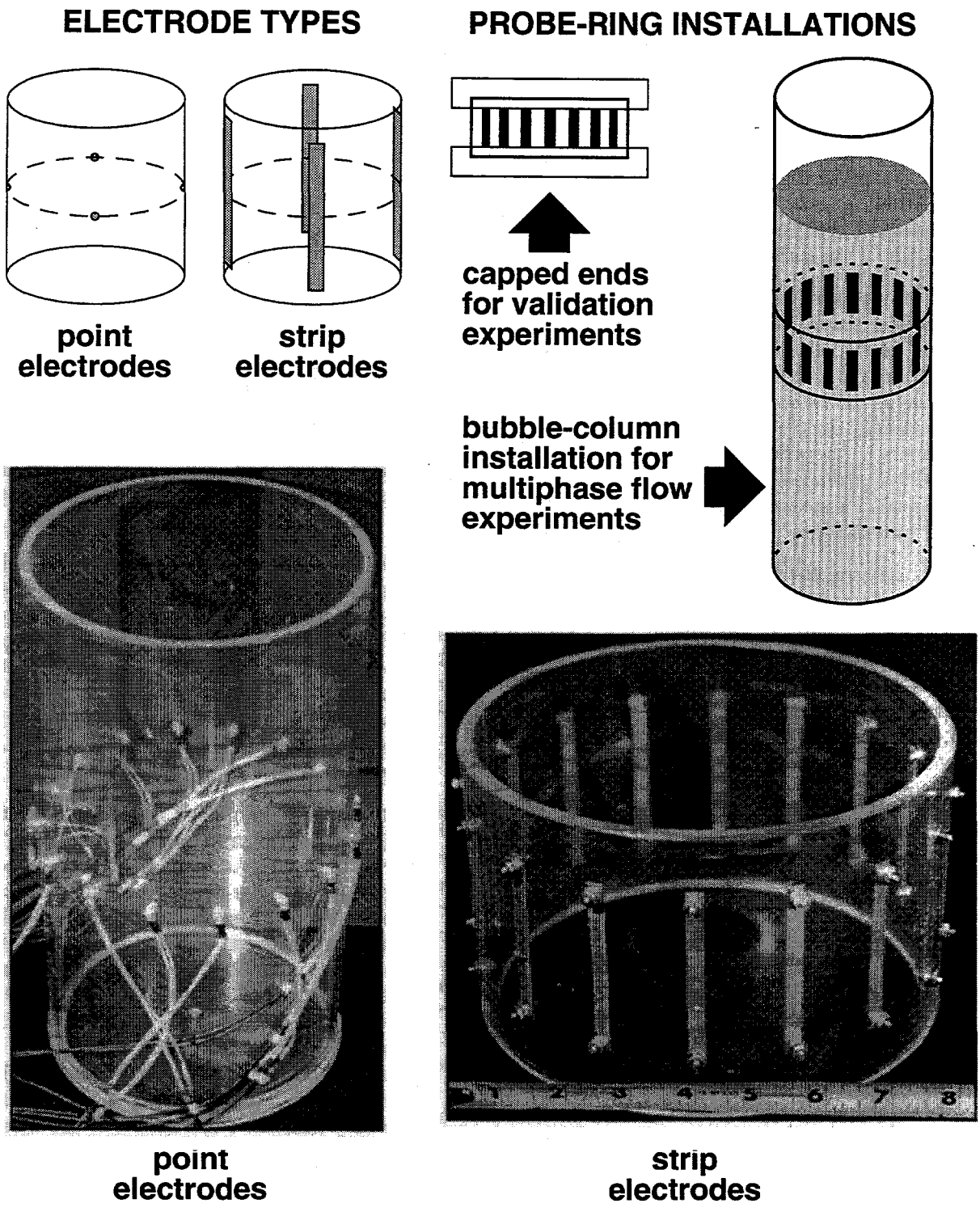


Figure 21. EIT strip and point electrodes and probe-ring installations.

### 2.4.2. EIT Reconstruction Algorithm: Overview

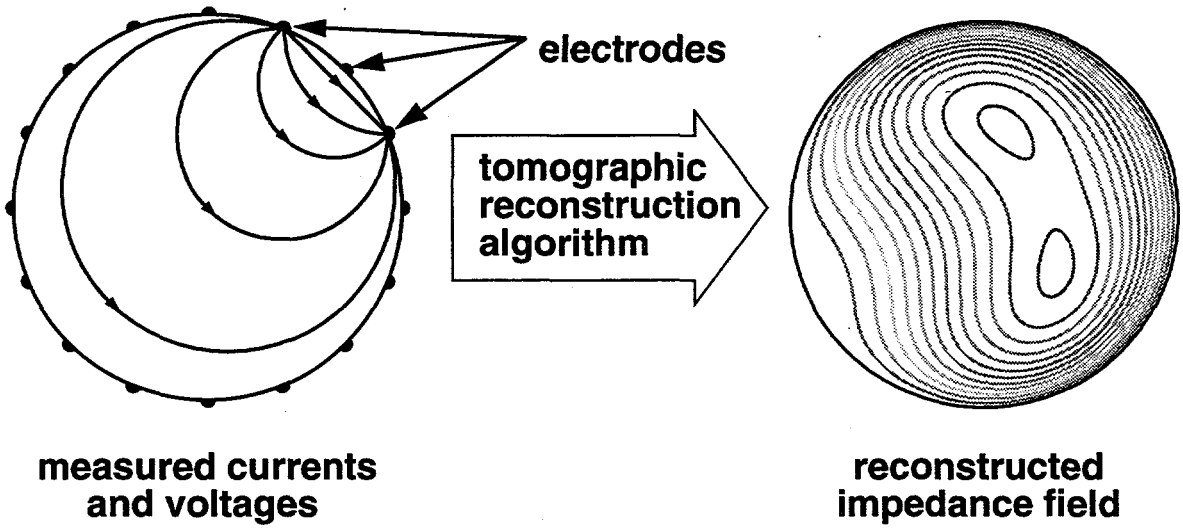


Figure 22. Schematic diagram of EIT.

As shown in Figure 22, for $N_e$ electrodes and $N_e(N_e-1)/2$ source-sink combinations, the goal of EIT is to use the $N_e^2(N_e-1)/2$ experimental voltages at the electrodes on the boundary to infer the impedance distribution in the interior. As previously indicated, reconstruction algorithms are considerably more complex for EIT than for GDT since the current paths through the material depend on the impedance distribution, whereas the gamma-photon paths through the material are known a priori to be straight lines. Thus, EIT tomographic reconstruction algorithms continue to be a subject of research (e.g Yorkey et al., 1987; Webster, 1990; Hua and Woo, 1990; Jones et al., 1993; Ceccio and George, 1996). In this study, the basic approach of Yorkey et al. (1987) has been followed. The medium is taken to be purely resistive (no capacitive effects), the conductivity spatial distribution is adjusted until the computational voltages most closely match the experimental voltages. The finite-element method (FEM) is used to discretize the voltage equation, and a Newton-Raphson (NR) method is used to minimize the rms difference between the computational and experimental voltages. This approach is developed generally and is implemented for two-dimensional situations and for three-dimensional situations with only radial variations in the conductivity field.

The physical model describing current flow in a purely resistive medium is the combination of steady charge conservation and Ohm's Law:

$$\nabla \cdot \mathbf{J} = 0, \tag{20}$$

$$\mathbf{J} = -\sigma \nabla V, \tag{21}$$

which yield

$$\nabla \cdot [\sigma \nabla V] = 0 \text{ in the domain,} \tag{22}$$

$$J_n = \mathbf{n} \cdot \mathbf{J} = -\mathbf{n} \cdot \sigma \nabla V \text{ on the boundary,} \tag{23}$$

where $V$ is the voltage (in V), $\sigma$ is the conductivity (in $\Omega^{-1}m^{-1}$), $\mathbf{J}$ is the current flux vector (in $A/m^2$), and $\mathbf{n}$ is the unit normal vector pointing outward on the domain boundary. The equation describing the voltage field is of the Laplace form, so proper boundary conditions require specifying either $V$ (Dirichlet condition) or $J_n$ (Neumann condition) everywhere on the boundary. For the situation considered here, $J_n$ is specified everywhere on the boundary. For this specification to be consistent, the total current flow out of (and into) the domain must be zero. This is satisfied since all of the current injected from one electrode into the domain is removed by another electrode. Since no voltage values are prescribed anywhere, a voltage field that is a solution to the above equations is unique only to within an arbitrary additive constant. To remove this ambiguity so that a solution can be obtained, the voltage must be specified at exactly one point in the domain. If the solution so obtained is offset by any arbitrary amount, the result is also a solution to the equations. Effectively, this means that each voltage solution has an arbitrary voltage offset as an adjustable parameter available to minimize the rms difference between the computational and experimental voltages.

Numerical solution of the Laplace equation describing the voltage field can be accomplished using a wide variety of standard methods. However, EIT has certain unusual features. The first is that the voltage equation is solved many times for the same conductivity field but with only slightly different boundary conditions, namely injection and withdrawal from different electrode pairs, as indicated previously. A numerical method should take advantage of this fact. The second feature is that the electrodes have small widths compared to the inter-electrode separation. It is therefore desirable to replace these small, distributed electrodes with infinitesimal electrodes (i.e. true mathematical points) in computations to avoid excessive resolution requirements in the vicinity of an electrode. These infinitesimal electrodes are taken to be two-dimensional points for strip electrodes and three-dimensional points for point electrodes. One difficulty with this replacement is that the electrode voltage scales inversely with the electrode width and formally becomes infinite (as does the current flux) if the distributed electrodes are replaced with mathematical points. Fortunately, this difficulty is circumvented in discretized forms of the voltage equation since the finite spatial resolution of the discretization prevents infinite values from occurring. Another difficulty with this replacement is that the voltages determined at current-carrying electrodes (the source and the sink) are no longer correctly determined. However, since they depend sensitively on the electrode geometry and the unknown contact resistance between the electrode and the conducting medium, the voltages at current-carrying electrodes should not be used when minimizing the rms difference between the computational and experimental voltages. This results in the loss of $N_e$ pieces of information, the unknown $N_e$ contact resistances.

It is convenient to nondimensionalize the physical quantities of interest in the following manner. Without loss of generality, assume that the current passing between each source-sink electrode pair is always the same and is described in terms of a current $I_e$ (in A) and a length scale $R$ (in m) by the current per unit length $I_e/R$ for infinitesimal strip electrodes and by the current $I_e$ for infinitesimal point electrodes. Also without loss of generality, assume that the medium under examination has an average conductivity on the order of the constant $\sigma_0$. Then the nondimensionalization presented in Table 1 is appropriate, and the symbols denoting dimensional quantities will be used to denote nondimensional quantities without exception for the remainder of this section.

Table 1. Nondimensionalization employed in EIT theoretical development.

| Quantity | Dimensional | Nondimensional |
|---|---|---|
| Position | $\mathbf{x}$ | $\mathbf{x}/R$ |
| Conductivity | $\sigma$ | $\sigma/\sigma_0$ |
| Current Flux | $J_n$ | $R^2 J_n / I_e$ |
| Voltage | $V$ | $\sigma_0 R V / I_e$ |

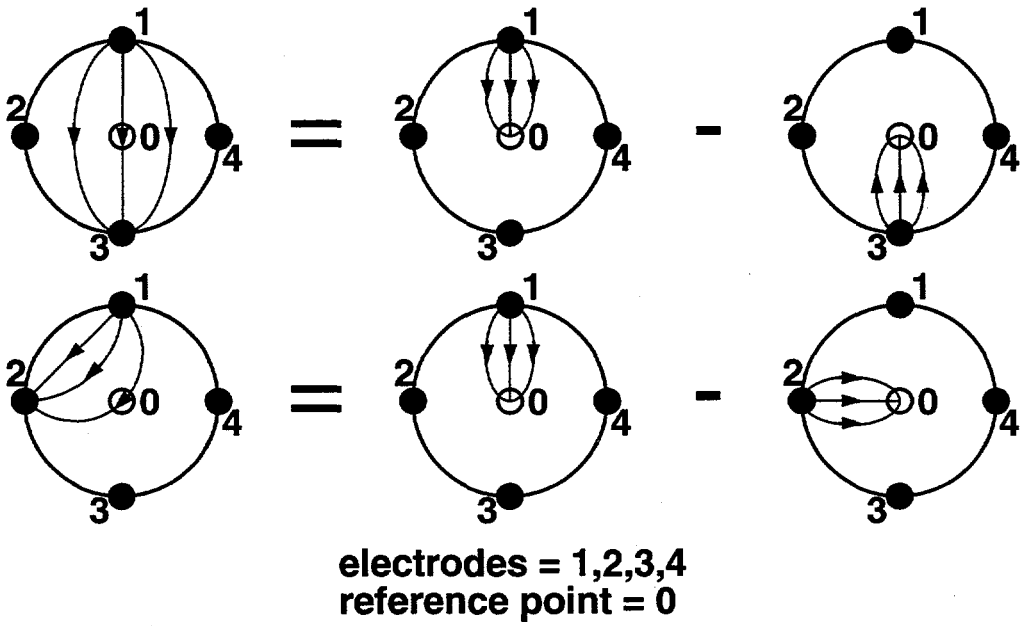


Figure 23. Linearity allows all EIT solutions to be built up from fewer solutions.

A considerable reduction of computational work can be achieved through application of the principle of linearity, as illustrated in Figure 23. As previously indicated, to determine the solution uniquely, the voltage must be specified at one point, henceforth called the reference point and denoted by "0". Suppose that the solution $V^{(k)}(\mathbf{x})$ corresponding to current injection at electrode $k$ and current withdrawal at the reference point has been determined for all electrodes. Then the solution $V^{(mn)}(\mathbf{x})$ for the EIT case with current injection and withdrawal at electrodes $m$ and $n$, respectively, can be built up using the linearity of the voltage equation (as shown in Figure 23) using the relation

$$V^{(mn)}(\mathbf{x}) = V^{(m)}(\mathbf{x}) - V^{(n)}(\mathbf{x}) . \tag{24}$$

Thus, for $N_e$ electrodes, only $N_e$ solutions are required to determine all $N_e(N_e-1)/2$ EIT solutions. This economy is also achieved for computation of the Jacobians discussed later.